Scrutiny of human lung infection by SARS-CoV-2 and associated human immune responses in humanized mice

Renren Sun[1,#], Zongzheng Zhao[2,#], Cong Fu[1], Yixin Wang[1,3], Zhendong Guo[2], Chunmao Zhang[2], Lina Liu[4], Cheng Zhang[5], Chang Shu[1], Jin He[1], Shucheng Hua[1,3,*], Yuwei Gao[2,*], Zheng Hu[1,*], Yong-Guang Yang[1,6,*]

[1] Key Laboratory of Organ Regeneration & Transplantation of Ministry of Education, and National-Local Joint Engineering Laboratory of Animal Models for Human Diseases, The First Hospital of Jilin University, Changchun 130062, China

[2] Changchun Veterinary Research Institute, Chinese Academy of Agricultural Sciences, Changchun 130122, China

[3] Department of Respiration, The First Hospital of Jilin University, Changchun 130061, China

[4] College of Veterinary Medicine, Jilin University, Changchun 130061, China

[5] College of Veterinary Medicine, Hebei Agricultural University, Baoding 071001, China

[6] International Center of Future Science, Jilin University, Changchun 130012, China

Running Head: Humanized mouse model of COVID-19

[#] These authors contributed equally to this work.

[*]Address correspondence to: yongg@jlu.edu.cn (Y.-G.Y.); zhenghu@jlu.edu.cn (Z.H.); shuchenghua@126.com (S-C.H.); gaoyuwei@gmail.com (Y-W. G.).

22 **Abbreviations:**

23 **HL**: human lung；**NSG-L**: NSG mice engrafted with human lung tissue；**HIS**: humanized
24 mice with human immune system；**HISL**: humanized mice with human immune system
25 and autologous human lung; **SARS-CoV-2**: severe acute respiratory syndrome
26 coronavirus 2; **COVID-19**: coronavirus disease 2019; **ACE2**: angiotensin-converting
27 enzyme 2; **IHC**: Immunohistochemistry; **RT-qPCR**: Real-time qPCR; **RNA-seq**: RNA
28 sequencing; **DEGs**: differentially expressed genes; **DO**: disease ontology; **GO**: gene
29 ontology;

30

31 **ABSTRACT**

32 There is an urgent need for animal models of COVID-19 to study immunopathogenesis
33 and test therapeutic intervenes. In this study we showed that NSG mice engrafted with
34 human lung (HL) tissue (NSG-L mice) could be infected efficiently by SARS-CoV-2,
35 and that live virus capable of infecting Vero cells was found in the HL grafts and multiple
36 organs from infected NSG-L mice. RNA-seq examination identified a series of
37 differentially expressed genes, which are enriched in viral defense responses, chemotaxis,
38 interferon stimulation, and pulmonary fibrosis between HL grafts from infected and
39 control NSG-L mice. Furthermore, when infecting humanized mice with human immune
40 system (HIS) and autologous HL grafts (HISL mice), the mice had bodyweight loss and
41 hemorrhage and immune cell infiltration in HL grafts, which were not observed in
42 immunodeficient NSG-L mice, indicating the development of anti-viral immune

43 responses in these mice. In support of this possibility, the infected HISL mice showed
44 bodyweight recovery and lack of detectable live virus at the later time. These results
45 demonstrate that NSG-L and HISL mice are susceptible to SARS-CoV-2 infection,
46 offering a useful *in vivo* model for studying SARS-CoV-2 infection and the associated
47 immune response and immunopathology, and testing anti-SARS-CoV-2 therapies.

48

49 **Keywords:** COVID-19, SARS-CoV-2, humanized mouse, lung infection

50

51 **Introduction**

52 The lack of animal models that can be easily used to model SARS-CoV-2 infection and
53 pathogenesis in biosafety level 3/4 facilities is an important drawback factor impeding
54 mechanistic understanding of coronavirus disease 2019 (COVID-19) pathogenesis and
55 test new anti-viral therapies(1). Although mice are the most popular and easily
56 handleable animal model, conventional murine models are not suitable for COVID-19
57 studies because most SARS-CoV-2 strains cannot use murine angiotensin-converting
58 enzyme 2 (ACE2) to invade mouse cells(2). Although human ACE2 transgenic mice
59 have been shown susceptible to SARS-CoV-2 infection(3, 4), this model overlooks other
60 proteins involved, such as transmembrane serine protease 2 (TMPRSS2) and CD147(5,
61 6). In addition, profound evolutionary divergences between mice and humans also
62 compromise their value to faithfully replicate viral infection process and the associated

63 disorders(7). Non-human primates are genetically close to human and can be infected by
64 SARS-CoV-2(8), however, their wide usage is intensively restrained due to their extreme
65 high cost and the need for complicated operating procedures especially in biosafety level
66 3/4 facilities. Thus, there is an urgent need for novel animal models that are easy to
67 handle and faithfully mimic human SARS-CoV-2 infection and the associated immune
68 responses.
69
70 Immune surveillance plays crucial roles in the control of viral infection and the
71 development of inflammatory syndromes, including pneumonia and cytokine storm in
72 COVID-19 patients(9). Previous studies of ours and other groups have shown that human
73 immune system (HIS) mice made by co-transplantation of human fetal thymic tissue
74 (under renal capsule) and $CD34^+$ fetal liver cells (FLCs, i.v.)(10, 11) could mount antigen
75 specific human T and antibody responses following immunization, viral infections or
76 transplantation(12-14). Recently, we generated a HIS mouse model with autologous
77 human lung (HL) tissues (referred to as HISL) by transplantation of both human fetal
78 lung (subcutaneous) and thymic tissues and $CD34^+$ FLCs, and validated its efficacy to
79 study human lung resident immunity and anti-viral response for H1N1 viral infection(15).
80 Herein, we further explored its application for SARS-CoV-2 infection investigation. We
81 found that these HISL mice could be infected by SARS-CoV-2 virus and develop

82 anti-viral immune responses, offering a convenient and useful *in vivo* model for
83 understanding COVID-19 pathogenesis and testing anti-SARS-CoV-2 interventions.
84
85 **Results and Discussion**
86 **Entry and replication of SARS-CoV-2 in HL xenografts in mice**
87 We first determined whether human lung tissue grafted in NOD/SCID IL2rg$^{-/-}$ (NSG)
88 mice can be infected by SARS-CoV-2. Briefly, NSG mice were implanted
89 subcutaneously with HL tissue (NSG-L mice), and subjected to infection via intra-HL
90 injection of SARS-CoV-2 or PBS (as controls) 6-8 weeks later. Immunohistochemistry
91 (IHC) examination confirmed human ACE2 protein expression throughout the HL
92 xenografts (Figure 1A). Real-time qPCR (RT-qPCR) analysis revealed that SARS-CoV-2
93 RNA was detected in HL and various mouse tissues including heart, liver, spleen, lung,
94 kidney, brain and intestine at days 1 and 3 following inoculation of 10^6 $TCID_{50}$
95 SARS-CoV-2, but not in NSG mice receiving subcutaneous injection of a similar number
96 of virus (Figure 1B), demonstrating SARS-CoV-2 infection and expansion in HL
97 xenografts. To confirm this observation, another cohort of NSG-L mice was intra-HL
98 inoculated with SARS-CoV-2 or mock. Again, viral copies were detected in HL at days 3,
99 5, 8, 14 and 21 after infection (Figure 1C). Importantly, 13 out of 14 HL homogenate
100 samples (except one at day 21) harvested from SARS-CoV-2-infected NSG-L mice at
101 days 3, 5, 8, 14, and 21 after infection retained the capability to re-infect Vero E6 cells *in*

102 *vitro*, demonstrating the existence of live SARS-CoV-2 in HL xenografts (Figure 1D).
103 However, viral inoculation did not lead to significant bodyweight loss (Figure 1E) or
104 detectable pathological changes in HL grafts (Figure 1F) or mouse tissues (Supporting
105 Information Figure 1), likely due to the immunodeficiency of NSG-L mice. This is in line
106 with previous reports that the complications in COVID-19 patients are largely
107 attributable to immune responses driven by SARS-CoV-2 infection(16).
108

109 **RNA-seq analysis for HL xenografts after SARS-CoV-2 infection**

110 To further understand the insight into SARS-CoV-2 infection induced changes in HL
111 cells, we analyzed the transcriptome by RNA-seq of HL samples from uninfected NSG-L
112 mice or infected NSG-L mice 5 and 21 days after SARS-CoV-2 inoculation. For day-5
113 HL grafts, a total of 4612 human genes were differentially expressed between two
114 samples, of which 2129 genes were significantly upregulated and 2483 genes were
115 downregulated ($|log2(FoldChange)| > 1$ & $padj < 0.05$) in SARS-CoV-2-infected
116 compared to uninfected HL grafts (Figure 2A left). For day-21 HL grafts, a total of 6488
117 human genes were differentially expressed between the two samples, of which 3311 and
118 3177 genes were significantly upregulated and downregulated ($|log2(FoldChange)| > 1$
119 & $padj < 0.05$), respectively in SARS-CoV-2-infected compared to uninfected HL grafts
120 (Figure 2A right). Many of these differentially expressed genes are associated with viral
121 defense responses, including NLRC5, MICB, APOBEC3D, APOBEC3G, IFI6, ISG15,

122 and IFITM3, which were markedly upregulated in infected HL grafts at days 5 and 21
123 compared to HL grafts from uninfected NSG-L mice (Figure 2B). Notability, HL grafts
124 from the infected NSG-L mice showed a great upregulation of viral infection-associated
125 chemokines (e.g., CCL11 and CXCL6 at day 5, and CCL19, CXCL19, CXCL13, CCL18
126 at day 21; Figure 2C) and interferon-stimulated genes (ISGs; e.g., IFIT1 and STAT1 at
127 day 5, and ISG15, IFITM1 and IFI27 at day 21; Figure 2D) compared to those from
128 non-infected NSG-L mice. Furthermore, SARS-CoV-2 infection induced intensive
129 upregulation of genes involved in pulmonary fibrosis at day 5 (e.g. CSF1, FASLG,
130 NLRP1) and day 21 (e.g. IGF2, IL18, MMP9) in infected HL grafts (Figure 2E),
131 providing a mechanistic explanation for the reported development of lung fibrosis, a
132 long-term and presumably irreversible complication of COVID-19 patients(17). Together,
133 these findings support the use of NSG-L mice as a convenient and useful *in vivo* platform
134 for modeling human lung infection with SARS-CoV-2 and testing anti-viral therapies.
135

136 **Development of antiviral immunity in HISL mice following SARS-CoV-2 infection**

137 We next examined SARS-CoV-2 infection in HISL mice with both HL and human
138 immunity. Briefly, HISL mice were constructed by transplantation of HL and thymic
139 tissues and $CD34^+$ cells, and subjected to SARS-CoV-2 infection after human immune
140 reconstitution was confirmed by measuring human immune cells in peripheral blood.
141 FACS analysis of PBMCs 14 weeks after humanization detected high levels of human

142 $CD45^+$ lymphohematopoietic cells composed of $CD3^+$ T cells (including both CD4 and
143 CD8 T cells), $CD20^+$ B cells and $CD33^+$ myeloid cells in HISL mice (Supporting
144 Information Figure 2A). Furthermore, human $CD45^+$ immune cells including $CD4^+$ T
145 cells, $CD20^+$ B cells and $CD11c^+$ dendritic cells were also detected in spleen and HL
146 grafts from these mice (Supporting Information Figure 2B). These HISL mice were
147 infected 3 weeks later with SARS-CoV-2 or mock as controls. Unlike NSG-L mice
148 (Figure 1), HISL mice showed a significant bodyweight loss after intra-HL SARS-CoV-2
149 infection, which returned to a level comparable to the control HISL mice by 21 days
150 (Figure 3A). No mortality was observed in HISL mice infected with SARS-CoV-2.
151 Furthermore, HL grafts from HISL mice that received SARS-CoV-2 (but not mock) had
152 hemorrhage at day 5, which was associated with increased infiltration by human $CD45^+$
153 cells, including $CD4^+$ T and $CD20^+$ B cells (Figure 3B). Although the levels of human T
154 and B cell infiltration in HL grafts became comparable between the two groups at day 21,
155 there were still significantly more human $CD33^+$ myeloid cells (Supporting Information
156 Figure 3A), including $CD11c^+$ cells (Supporting Information Figure 3B), in HL grafts in
157 SARS-CoV-2-infected than mock infected mice, which is in line with previous reports
158 for patients(18, 19). No significant difference was detected for any human immune cell
159 populations in WBCs, including $CD3^+$ T, $CD20^+$ B, $CD33^+$ myeloid, and $CD56^+$ NK cells
160 between SARS-CoV-2- and mock-infected mice at day 21 (Supporting Information
161 Figure 3C). Viral copies were detected by RT-qPCR in all HL samples (except one at day

162 21) from SARS-CoV-2-infected HISL mice, but not those from the control HISL mice
163 (Figure 3C). However, in contrast to HL homogenates from infected NSG-L mice (Figure
164 1), HL homogenate samples from most infected HISL mice harvested at day 5 (5 out 6)
165 and day 21 (5 out 6) failed to infect Vero E6 cells *in vitro* (Figure 3D), indicating an
166 efficient elimination of live SARS-CoV-2 by human immune system in these mice.
167 Together, these results suggest that the clinical symptoms were caused mainly by
168 inflammation/immune responses, but not viral invasion directly, supporting the use of
169 HISL mice to study COVID-19 pathogenesis and anti-SARS-CoV-2 immunotherapy.
170

171 **Concluding Remarks**

172 In this study, we established a humanized mouse model carrying human lung tissue and
173 autologous immune system, which can be easily constructed and comfortably used in
174 ABSL-3 laboratories. We found that these humanized mice are susceptible to infection by
175 SARS-CoV-2 and develop disease-associated lung injury. Although not capable of
176 modeling upper respiratory or systemic infection/manifestations, as only the HL
177 xenograft is susceptible to SARS-CoV-2 in these mice, this model is still useful as the
178 only currently available model that permits *in vivo* assessment of human immune
179 responses against SARS-CoV-2 infection. Therefore, the HISL humanized mouse model
180 offers a convenient and powerful *in vivo* model for evaluating the immunopathology of
181 COVID-19 and the efficacy of anti-viral immunotherapies, such as vaccination.

182

183 **Material and methods**

184 **Mice and human tissues**

185 NOD-Prkd^{cem26Cd52}Il2rg^{em26Cd22}/Nju (referred to as NSG) mice were purchased from
186 Nanjing Biomedical Research Institute of Nanjing University. All mice were housed in a
187 specific pathogen-free (SPF) microisolator environment and used between 6-8 weeks of
188 age. Discard human fetal samples of gestational age of 17-22 weeks were obtained with
189 informed consent at the First Hospital of Jilin University. Human fetal thymic and lung
190 tissues were cut into small pieces with a diameter of around 1 mm or 5 mm, respectively,
191 and CD34$^+$ cells were purified from fetal liver cells (FLCs) by magnetic-activated cell
192 sorting (MACS; with a purity of >90% confirmed by FACS). The human tissues and cells
193 were cryopreserved in liquid nitrogen until use.

194 **NSG-L mouse and HISL humanized mouse model construction**

195 NSG-L mice were made by subcutaneous implantation of human fetal lung tissue
196 (approximately 5 mm in diameter). HISL humanized mice were made by implantation of
197 human fetal thymic tissue (around 1 mm in diameter; under the renal capsule) and lung
198 tissue (5 mm in diameter; subcutaneously) in NSG mice that pre-conditioned with 1.75
199 Gy total body irradiation (TBI; Rad Source RS2000-225, USA), followed by intravenous
200 injection of 1-2$\times 10^5$ human CD34$^+$ FLCs (given 6-8 hours after TBI).

201 **Flow cytometric analysis**

202 Mouse PBMCs were prepared using density gradient centrifugation with Histopaque
203 1077 (Sigma-Aldrich, St. Louis, MO). Human immune cell reconstitution in humanized
204 mice were determined by flow cytometry using following fluorochrome-conjugated
205 antibodies: anti-human CD45, CD3, CD4, CD8, CD20, CD33, CD56; anti-mouse CD45
206 and Ter119 (BD Biosciences, USA). Examination was performed on a Cytek Aurora
207 (Cytek Biosciences, USA) and data were analyzed using the FlowJo software version
208 10.6.2. Dead cells were excluded from the analysis by gating out propidium iodide
209 retaining cells.

210 **SARS-CoV-2 virus preparation and titer determination**

211 SARS-CoV-2 (BetaCoV/Beijing/IME-BJ05-2020) was proliferated in Vero E6 cells,
212 which are maintained in Dulbecco's modified Eagle's medium (DMEM; Invitrogen,
213 Carlsbad, CA, USA) with supplemented 2% fetal bovine serum (FBS; Gibco, Auckland,
214 New Zealand). Viral titers were determined using a standard 50% tissue culture infection
215 dose ($TCID_{50}$) assay.

216 **Mouse experiments**

217 NSG-L or HISL mice were anesthetized with isoflurane and injected with 100 μl of 10^6
218 $TCID_{50}$ of SARS-CoV-2 or PBS into the human lung (HL) graft. The mice were followed
219 for bodyweight changes, and euthanized for measuring viral particles and histological
220 changes in HL grafts and tissues at indicated time points.

221 **RNA extraction and RT-qPCR**

222 Total RNA was extracted from tissues homogenates using the RNeasy Mini Kit (Qiagen,
223 Hilden, Germany), and viral RNA loads were determined by a SARS-CoV-2 RNA
224 detection kit (Shenzhen Puruikang Biotech, China). The viral RNA loads for the target
225 SARS-CoV-2 N gene was normalized to the standard curve obtained by using a plasmid
226 containing the full-length cDNA of the SARS-CoV-2 N gene. The reactions were
227 performed with CFX96 system (BIO-RAD, USA) according to the following protocol:
228 50 °C for 20 min for reverse transcription, followed by 95 °C for 3 min and then 45
229 cycles of 95 °C for 5 s, 56 °C for 45 s. Results were presented as log10 numbers of
230 genome equivalent copies per gram of sample.

231 **Histology**

232 Tissues were embedded in paraffin, and sectioned (2.5 μm) for H&E and
233 immunohistochemistry (IHC) examination. For IHC, tissue sections were firstly stained
234 with monoclonal anti-human CD45 (DAKO, 2B11+PD7/26), CD20 (DAKO, L26), CD4
235 (ABclonal; ARC0328), or CD11c (Abcam; EP1347Y), ACE2 (Abcam; EPR4435(2))
236 antibodies, and the immunoreactivity was detected with UltraSensitiveTM
237 Streptavidin-Peroxidase Kit (KIT-9710, Mai Xin, China) according to the manufacturer's
238 protocol.

239 **RNA-seq**

240 Total RNA was polyA-selected, fragmented and the samples were examined on an
241 Illumina Novaseq6000 machine, yielding an average of 22 million uniquely aligned

242 paired-end 150-mer reads per sample. Reads were aligned with STAR RNA-seq aligner
243 (Version 2.7.3a) using the UCSC/hg38 genome assembly and transcript annotation(20).
244 Expression levels were calculated as Fragments per Kilobase of transcript per Million
245 reads (FPKM) using Cufflinks software(21). Differential expression analysis was
246 performed using Cuffdiff (version 2.2.1.Linux_x86_64)(21). In each analysis, genes with
247 thresholds of |log 2 (foldchange)| > 1, *p adj* < 0.05 and a mean FPKM value of more than
248 5 were tested. "Cluster Profiler" package (Release 3.16.1)(22) and "DOSE" package
249 (Release 3.14.0)(23) in R software (version 4.0.2) was used for functional enrichment
250 analysis, and GO biological processes terms at the significant level (*q-value* < 0.05) were
251 employed.

252 **Statistical analysis**

253 Data were analyzed using GraphPad Prism 8 software (San Diego, CA, USA) and
254 presented as mean values ± SEM. The results were compared statistically using unpaired
255 two-tailed Student's t test and two-way analysis of variance (ANOVA), and a p value of
256 ≤ 0.05 was considered significant.

257

258 **Data availability statement:** RNA-seq data have been deposited into the National
259 Center for Biotechnology Information (NCBI) Gene Expression Omnibus (GEO)
260 database under accession numbers GSE175900.

261 **Conflict of interest:** The authors declare that they have no competing financial interests.

262 **Ethics approval statement for human and animal studies:** Protocols involved in the
263 use of human samples and animals were reviewed and approved by the Institutional

264 Review Board and Institutional Animal Care and Use Committee of the First Hospital of
265 Jilin University, and all experiments with SARS-CoV-2 (COVID-19) were performed in
266 biosecurity level 3 laboratory according to the protocols approved by the Changchun
267 Veterinary Research Institute, Chinese Academy of Agricultural Sciences.

268 **Author contributions:** Z.H., Y-W. G., S-C.H, Y-G.Y. conceived the study; R-R.S.,
269 Z-Z.Z., Y-X.W., C.S., J.H. performed the experiments; C.F. contributed to RNA-seq data
270 analysis; Z.H., Y-W.G., S-C.H. supervised the work; Z.H., R-R.S., Z-Z.Z., C.F. Y-G.Y.
271 analyzed the data and wrote the manuscript; all authors edited and approved the
272 manuscript.

273 **Acknowledgements**

274 This work was supported by grants from the Strategic Priority Research Program of the
275 Chinese Academy of Sciences (XDA16030303), Chinese MOST (2017YFA0104402)
276 and NSFC (91742107, 81870091, 91642208, 82001697 and 81941008), Science
277 development project of Jilin province (20190201295JC and 20200703012ZP), and
278 special grants for COVID-19 research of Jilin province (20200901006SF).

279 **References**

280 1. Muñoz-Fontela C, Dowling WE, Funnell SG, Gsell P-S, Riveros-Balta AX,
281 Albrecht RA, Andersen H, Baric RS, Carroll MW, Cavaleri M. 2020. Animal
282 models for COVID-19. Nature 586:509-515.

283 2. Wang Q, Zhang Y, Wu L, Niu S, Song C, Zhang Z, Lu G, Qiao C, Hu Y, Yuen K-Y.
284 2020. Structural and functional basis of SARS-CoV-2 entry by using human

285 ACE2. Cell 181:894-904. e9.

286 3. Bao L, Deng W, Huang B, Gao H, Liu J, Ren L, Wei Q, Yu P, Xu Y, Qi F. 2020.
287 The pathogenicity of SARS-CoV-2 in hACE2 transgenic mice. Nature
288 583:830-833.

289 4. Zheng J, Wong L-YR, Li K, Verma AK, Ortiz ME, Wohlford-Lenane C, Leidinger
290 MR, Knudson CM, Meyerholz DK, McCray PB. 2021. COVID-19 treatments and
291 pathogenesis including anosmia in K18-hACE2 mice. Nature 589:603-607.

292 5. Qiao J, Li W, Bao J, Peng Q, Wen D, Wang J, Sun B. 2020. The expression of
293 SARS-CoV-2 receptor ACE2 and CD147, and protease TMPRSS2 in human and
294 mouse brain cells and mouse brain tissues. Biochemical and Biophysical Research
295 Communications 533:867-871.

296 6. Wang K, Chen W, Zhang Z, Deng Y, Lian J-Q, Du P, Wei D, Zhang Y, Sun X-X,
297 Gong L. 2020. CD147-spike protein is a novel route for SARS-CoV-2 infection to
298 host cells. Signal transduction and targeted therapy 5:1-10.

299 7. Perrin S. 2014. Preclinical research: Make mouse studies work. Nature News
300 507:423.

301 8. Blair RV, Vaccari M, Doyle-Meyers LA, Roy CJ, Russell-Lodrigue K, Fahlberg M,
302 Monjure CJ, Beddingfield B, Plante KS, Plante JA. 2021. Acute Respiratory
303 Distress in Aged, SARS-CoV-2–Infected African Green Monkeys but Not Rhesus
304 Macaques. The American journal of pathology 191:274-282.

305 9. Sariol A, Perlman S. 2020. Lessons for COVID-19 immunity from other
306 coronavirus infections. Immunity.
307 10. Lan P, Wang L, Diouf B, Eguchi H, Su H, Bronson R, Sachs DH, Sykes M, Yang
308 Y-G. 2004. Induction of human T-cell tolerance to porcine xenoantigens through
309 mixed hematopoietic chimerism. Blood 103:3964-3969.
310 11. Lan P, Tonomura N, Shimizu A, Wang S, Yang Y-G. 2006. Reconstitution of a
311 functional human immune system in immunodeficient mice through combined
312 human fetal thymus/liver and CD34+ cell transplantation. Blood 108:487-492.
313 12. Tonomura N, Habiro K, Shimizu A, Sykes M, Yang Y-G. 2008. Antigen-specific
314 human T-cell responses and T cell–dependent production of human antibodies in a
315 humanized mouse model. Blood, The Journal of the American Society of
316 Hematology 111:4293-4296.
317 13. Tonomura N, Shimizu A, Wang S, Yamada K, Tchipashvili V, Weir GC, Yang YG.
318 2008. Pig islet xenograft rejection in a mouse model with an established human
319 immune system. Xenotransplantation 15:129-135.
320 14. Brainard DM, Seung E, Frahm N, Cariappa A, Bailey CC, Hart WK, Shin H-S,
321 Brooks SF, Knight HL, Eichbaum Q. 2009. Induction of robust cellular and
322 humoral virus-specific adaptive immune responses in human immunodeficiency
323 virus-infected humanized BLT mice. Journal of virology 83:7305-7321.
324 15. Wang Y, Wang L, Fu C, Wang X, Zuo S, Shu C, Shan Y, He J, Zhou Q, Li W.

325 2021. Exploration of Human Lung-Resident Immunity and Response to
326 Respiratory Viral Immunization in a Humanized Mouse Model. The Journal of
327 Immunology.
328 16. Vardhana SA, Wolchok JD. 2020. The many faces of the anti-COVID immune
329 response. Journal of Experimental Medicine 217.
330 17. Grillo F, Barisione E, Ball L, Mastracci L, Fiocca R. 2021. Lung fibrosis: an
331 undervalued finding in COVID-19 pathological series. The Lancet Infectious
332 Diseases 21:e72.
333 18. Szabo PA, Dogra P, Gray JI, Wells SB, Connors TJ, Weisberg SP, Krupska I,
334 Matsumoto R, Poon MM, Idzikowski E. 2021. Longitudinal profiling of
335 respiratory and systemic immune responses reveals myeloid cell-driven lung
336 inflammation in severe COVID-19. Immunity 54:797-814. e6.
337 19. Nienhold R, Ciani Y, Koelzer VH, Tzankov A, Haslbauer JD, Menter T, Schwab
338 N, Henkel M, Frank A, Zsikla V. 2020. Two distinct immunopathological profiles
339 in autopsy lungs of COVID-19. Nature communications 11:1-13.
340 20. Dobin A, Davis CA, Schlesinger F, Drenkow J, Zaleski C, Jha S, Batut P,
341 Chaisson M, Gingeras TR. 2013. STAR: ultrafast universal RNA-seq aligner.
342 Bioinformatics 29:15-21.
343 21. Trapnell C, Williams BA, Pertea G, Mortazavi A, Kwan G, Van Baren MJ,
344 Salzberg SL, Wold BJ, Pachter L. 2010. Transcript assembly and quantification by

345 RNA-Seq reveals unannotated transcripts and isoform switching during cell
346 differentiation. Nature biotechnology 28:511-515.
347 22. Yu G, Wang L-G, Han Y, He Q-Y. 2012. clusterProfiler: an R package for
348 comparing biological themes among gene clusters. Omics: a journal of integrative
349 biology 16:284-287.
350 23. Yu G, Wang L-G, Yan G-R, He Q-Y. 2015. DOSE: an R/Bioconductor package
351 for disease ontology semantic and enrichment analysis. Bioinformatics
352 31:608-609.
353
354

355 **Figure legends**

356 **Figure 1 SARS-CoV-2 infection of HL xenografts in NSG mice.** NSG-L mice were
357 subjected to SARS-CoV-2 infection (10^6 $TCID_{50}$ given by intra-HL injection) 6-8 weeks
358 after HL transplantation. Data from two independent experiments are presented, in which
359 NSG mice receiving subcutaneous injection of SARS-CoV-2 (**B**) or NSG-L mice
360 receiving intra-HL injection of PBS (**C-F**) were used as controls, respectively. **(A)**
361 Representative IHC images of HL xenografts (up, isotype; down, human ACE2). **(B)**
362 Viral copies in the indicated tissues examined by RT-qPCR 1 (n=2 and 1 for HL-infected
363 and control groups, respectively) or 3 (n=1 per group) days after infection. **(C-F)** Viral
364 RNA copies examined by RT-qPCR (**C**) and titers measured by Vero E6 cells (**D**) in HL
365 xenografts, and bodyweight changes (**E**) at the indicated time points (n=3 per group); (**F**)
366 Representative H&E images of HL xenografts at day 5 after intra-HL injection of PBS
367 (left) or SARS-CoV-2 (right).

368

369 **Figure 2 RNA-seq analysis for HL grafts from NSG-L mice after SARS-CoV-2**
370 **infection.** HL grafts injected with 10^6 $TCID_{50}$ SARS-CoV-2 virus were harvested from
371 NSG-L mice for RNA-seq examination at day 5 and 21 after infection; Naïve HL graft
372 without infection was used as control. **(A)** Volcano plot showing DEGs of HL grafts for
373 SARS-CoV2-infected at day 5 (left) or day 21 (right) and non-infection control from
374 NSG-L mice. The data for all genes are plotted as log2 fold change versus the −log10 of

375 the adjusted p-value. **(B-E)** Heatmaps of RNA-seq expression Z-scores computed for
376 selected genes that are differentially expressed ($p\ adj < 0.05$, |log 2 (foldchange)| > 1)
377 between 3 pairwise comparisons (L_E5 vs L_E21, Lung vs L_E5, Lung vs L_E21). (**B**)
378 DEGs under GO term "defense response to virus" (BP GO: 0051607); (**C**) Chemokines;
379 (**D**) Interferon-stimulated genes; **(E)** DEGs under DO term "Pulmonary Fibrosis"
380 (DOID:3770).
381
382 **Figure 3 HISL mice are susceptible for SARS-CoV-2.** HISL mice were infected at
383 week 17 post-humanization with mock or 10^6 $TCID_{50}$ SARS-CoV-2 into HL. (**A**)
384 Bodyweight changes of HISL mice infected with SARS-CoV-2 (n=6) or mock (n=4). (**B**)
385 Representative H&E and IHC images of HL sections of HISL mice infected with
386 SARS-CoV-2 (n=6) or mock (n=4) at day 5. (**C-D**) Mice were euthanized at days 2, 5,
387 and 21 post-infection, and SARS-CoV-2 viral copies (**C**) and viral titers (**D**) in HL were
388 examined (each symbol represents an individual animal). $*P < 0.05$.

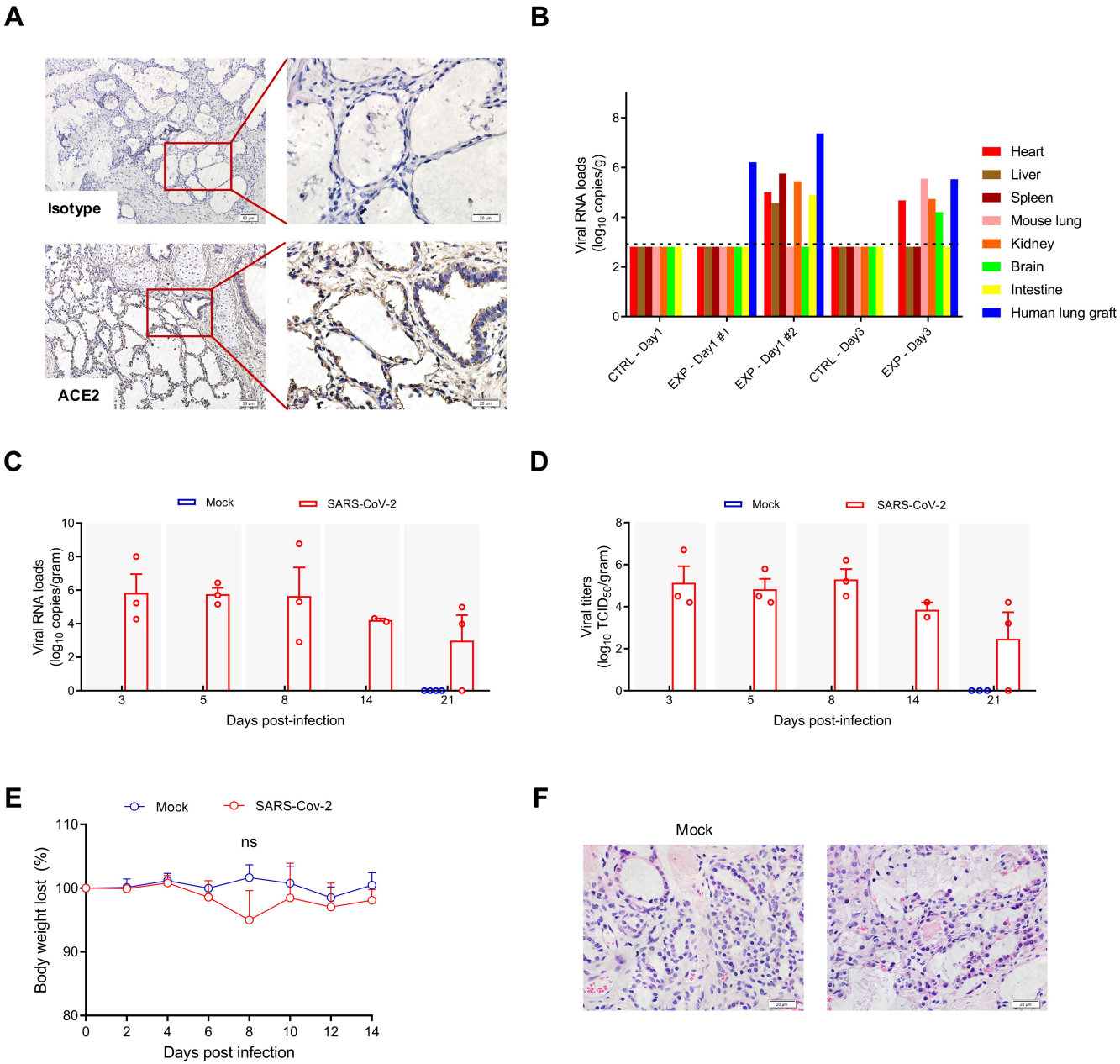
A
Isotype
ACE2
B
Viral RNA loads
(log10 copies/g)
0
2
4
6
8
CTRL - Day1
EXP - Day1 #1
EXP - Day1 #2
CTRL - Day3
EXP - Day3
Heart
Liver
Spleen
Mouse lung
Kidney
Brain
Intestine
Human lung graft
C
Mock
SARS-CoV-2
Viral RNA loads
(log10 copies/gram)
0
2
4
6
8
10
3
5
8
14
21
Days post-infection
D
Mock
SARS-CoV-2
Viral titers
(log10 TCID50/gram)
0
2
4
6
8
3
5
8
14
21
Days post-infection
E
Mock
SARS-Cov-2
ns
Body weight lost (%)
80
90
100
110
0
2
4
6
8
10
12
14
Days post infection
F
Mock

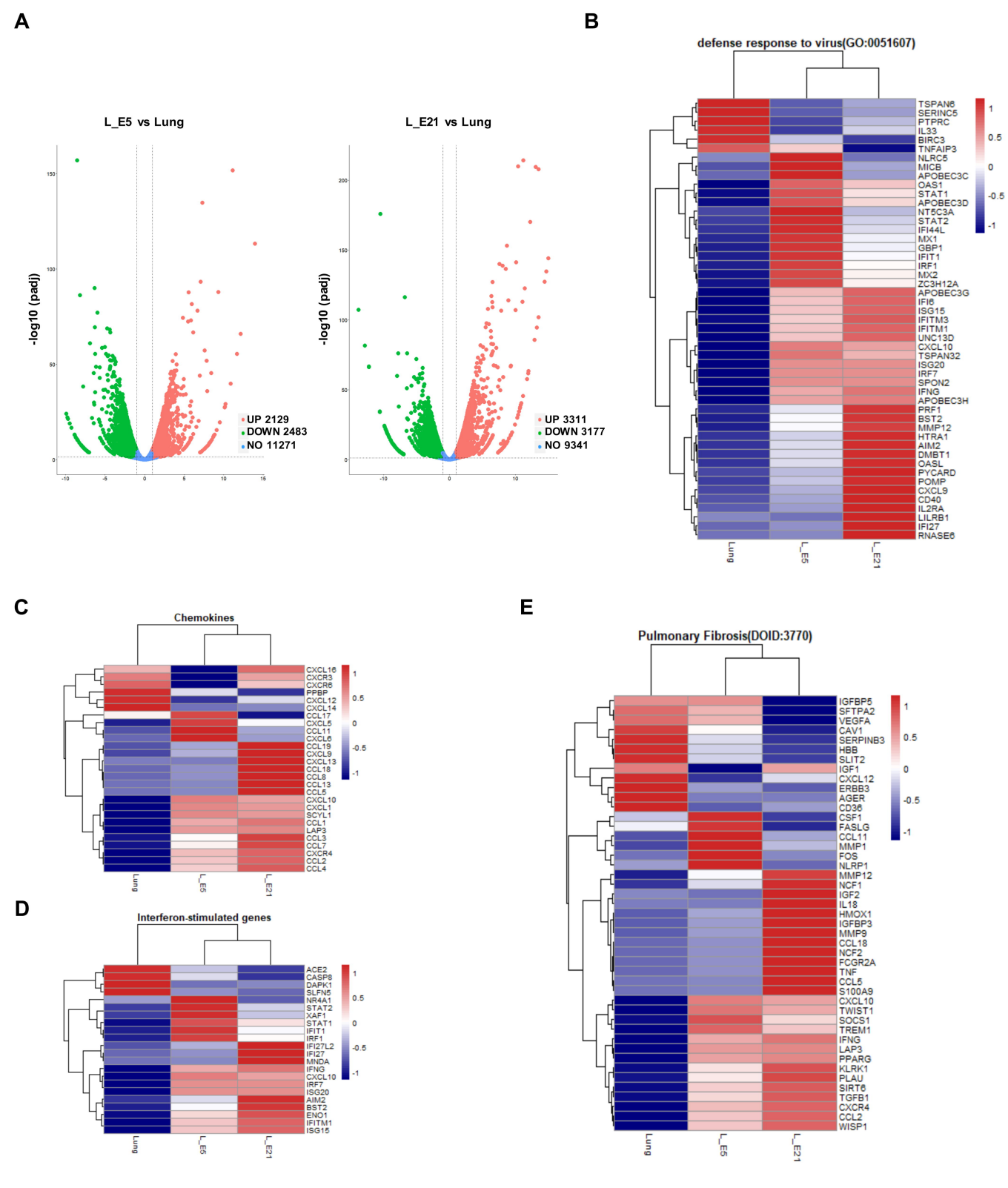
A
L_E5 vs Lung
-log10 (padj)
UP 2129
DOWN 2483
NO 11271
L_E21 vs Lung
-log10 (padj)
UP 3311
DOWN 3177
NO 9341
B
defense response to virus(GO:0051607)
TSPAN6
SERINC5
PTPRC
IL33
BIRC3
TNFAIP3
NLRC5
MICB
APOBEC3C
OAS1
STAT1
APOBEC3D
NT5C3A
STAT2
IFI44L
MX1
GBP1
IFIT1
IRF1
MX2
ZC3H12A
APOBEC3G
IFI6
ISG15
IFITM3
IFITM1
UNC13D
CXCL10
TSPAN32
ISG20
IRF7
SPON2
IFNG
APOBEC3H
PRF1
BST2
MMP12
HTRA1
AIM2
DMBT1
OASL
PYCARD
POMP
CXCL9
CD40
IL2RA
LILRB1
IFI27
RNASE6
Lung
L_E5
L_E21
C
Chemokines
CXCL16
CXCR3
CXCR6
PPBP
CXCL12
CXCL14
CCL17
CXCL5
CCL11
CXCL6
CCL19
CXCL9
CXCL13
CCL18
CCL8
CCL13
CCL5
CXCL10
CCL1
SCYL1
CCL1
LAP3
CCL3
CCL7
CXCR4
CCL2
CCL4
Lung
L_E5
L_E21
D
Interferon-stimulated genes
ACE2
CASP8
DAPK1
SLFN5
NR4A1
STAT2
XAF1
STAT1
IFIT1
IRF1
IFI27L2
IFI27
MNDA
IFNG
CXCL10
IRF7
ISG20
AIM2
BST2
ENO1
IFITM1
ISG15
Lung
L_E5
L_E21
E
Pulmonary Fibrosis(DOID:3770)
IGFBP5
SFTPA2
VEGFA
CAV1
SERPINB3
HBB
SLIT2
IGF1
CXCL12
ERBB3
AGER
CD36
CSF1
FASLG
CCL11
MMP1
FOS
NLRP1
MMP12
NCF1
IGF2
IL18
HMOX1
IGFBP3
MMP9
CCL18
NCF2
FCGR2A
TNF
CCL5
S100A9
CXCL10
TWIST1
SOCS1
TREM1
IFNG
LAP3
PPARG
KLRK1
PLAU
SIRT6
TGFB1
CXCR4
CCL2
WISP1
Lung
L_E5
L_E21

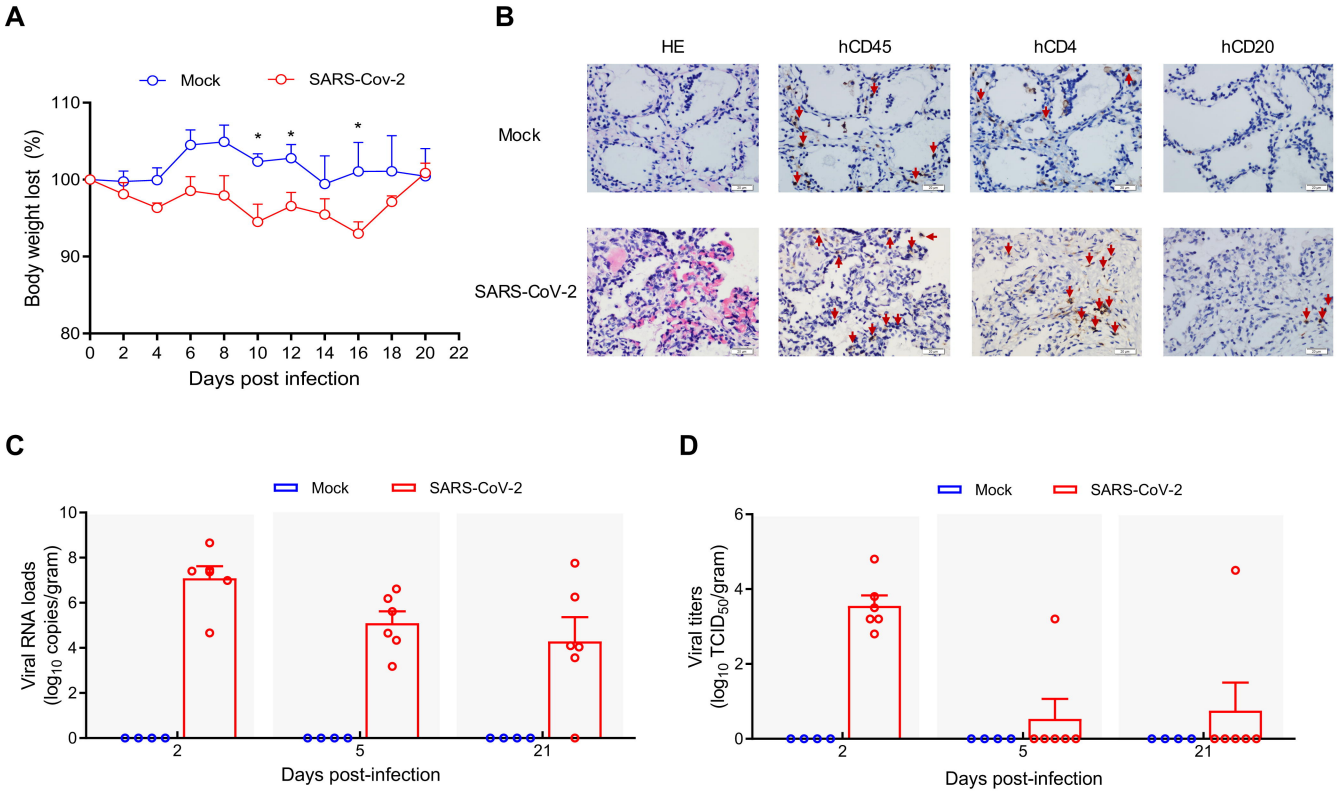
A
Mock
SARS-Cov-2
Body weight lost (%)
110
100
90
80
0 2 4 6 8 10 12 14 16 18 20 22
Days post infection
B
HE
hCD45
hCD4
hCD20
Mock
SARS-CoV-2
C
Mock
SARS-CoV-2
Viral RNA loads
(log10 copies/gram)
10
8
6
4
2
0
2
5
21
Days post-infection
D
Mock
SARS-CoV-2
Viral titers
(log10 TCID50/gram)
6
4
2
0
2
5
21
Days post-infection